Colloid Polym Sci (2002) 280: 736–743
DOI 10.1007/s00396-002-0679-y

ORIGINAL CONTRIBUTION

Tamás Haraszti
Imre Dékány

Light scattering and the fractal properties of hydrophilic and hydrophobic SiO_2 aggregates in ethanol–toluene binary mixtures

Received: 4 November 2001
Accepted: 18 February 2002
Published online: 18 April 2002

T. Haraszti
Department of Colloid Chemistry,
University of Szeged, 6720 Szeged,
Aradi vt. t. 1, Hungary

I. Dékány (✉)
Nanostructured Materials Research Group
of Hungarian Academy of Sciences,
University of Szeged, 6720 Szeged,
Aradi vt. t. 1, Hungary
E-mail: i.dekany@chem.u-szeged.hu
Tel.: +36-62-544211
Fax: +36-62-544042

Abstract The aggregation properties of silica particles with hydrophilic or hydrophobic surface were investigated in ethanol–toluene binary mixtures. The interaction between the particles was altered by changing the composition of the liquid mixture from pure ethanol to pure toluene. The kinetic stability of the sols decreased with increasing concentration of toluene for the hydrophilic particles and with increasing concentration of ethanol for the hydrophobic particles. The decreasing stability correlated well with the variation of the second virial coefficient determined from turbidity measurements and the concentration dependence of the mass fractal dimension, $d(c, x_1)$, determined from static light scattering. This latter parameter indicated that the aggregation structure is dominated by chainlike aggregates ($d \approx 1$) for the more stable suspensions and more space filling structures ($d \approx 3$) for the less stable systems.

Keywords Binary mixtures · Fractal structure · Second virial coefficient · Colloid stability · Static light scattering

Introduction

The stability of particles in suspensions is an important topic in colloid science. However, in everyday practice, the chemical composition of the samples is rather complex and the size and shape of the particles is heterogeneous. Therefore, model systems have to be constructed, in which the interparticle interaction and the colloid stability can be studied. Such studies can be performed in two different directions using the fact that in aqueous electrolyte solutions the Derjaguin–Landau–Verwey–Overbeek interactions and in organic solvents the van der Waals interactions dominate.

In our current study we focus on organic solvents. In the presence of a complex, multicomponent medium, the interaction between the particles can be significantly different from that in the pure components, when adsorption occurs [1, 2, 3, 4, 5, 6, 7, 8, 9, 10, 11]. To obtain useable model results, we applied a mixture of two organic solvents, such as benzene–*n*-heptane, methanol–benzene, and ethanol–cyclohexane. We can correlate the stability of the suspension, the adsorption excess isotherms, the Bingham yield stress, the energy of separation, the enthalpy of wetting, the excess free energy, model calculations for the van der Waals potentials, and different size parameters obtained in small-angle X-ray scattering measurements [4, 5, 6, 7, 8, 9, 10, 11]. The experiments were performed on different silica particles – pyrolytic and Stöber silica [12] – with two types of surfaces: one has the original silica surface with more hydrophilic characteristics, such as silicon oxide; the other is modified by long-chain alcohols (e.g., stearyl alcohol). The latter sample has hydrophobic character from a wetting point of view. For clarity, the particles without and with surface modification are referred to in the following as hydrophilic and hydrophobic, respectively.

Static light scattering and turbidimetry measurements were applied to determine the optical density, the radius of gyration, R_g, and the second virial coefficient, B_2 [13,

14,15]. Vrij and coworkers [14, 15] found that turbidimetric measurement was well applicable for concentrated suspensions, where the effect of multiple scattering is not negligible anymore. R_g and B_2 were derived from calculations analogous to those following the method of Zimm for polymers [14, 15, 16]. The second virial coefficient can be related to the osmotic pressure in the same way as for polymers and can be directly related to the interparticle interaction potential [16].

In this present work we investigated the application of static and dynamic light scattering and turbidimetry on suspensions of silica particles in a binary organic mixture (ethanol–toluene). Our aim was to understand how the parameters characteristic of the interaction and the structure of the particle aggregates vary as the interaction is controlled through changing the composition of the medium.

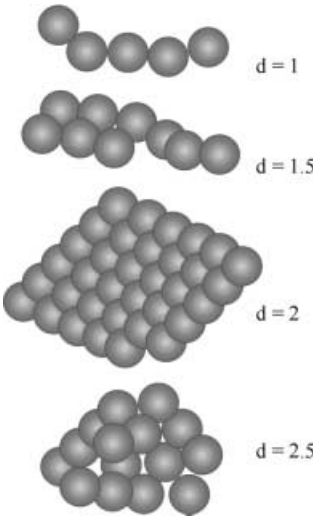

Fig. 1. Aggregates with different mass fractal dimensions, d

Theoretical background

An object with a fractal structure in general is considered to show a surface area or mass that scales with a noninteger power of the (largest) characteristic size of the object. For particle aggregates, the mass of the aggregate is proportional to the largest size, R, to the power of the fractal dimension, d (Eq. 1). The characteristic power, d, is commonly called the mass fractal dimension:

$$m(R) \propto R^d. \tag{1}$$

The value of d for regular objects (sphere, cube, etc.) is an integer number, and for a fractal-type object it is a real number between 1 and 3, depending on the structure of the aggregate [17, 18, 19, 20, 22]. The scheme in Fig. 1 presents a trivial meaning of $d = 1.0$ (a line), 2.0 (a plane), or close to 3.0 (a space-filling structure). It is shown in many publications that the scattered intensity of a mass fractal-type structure is proportional to the inverse power of the scattering vector, h (Eq. 2) [17, 18, 19, 20, 22]:

$$I \propto h^{-d}, \tag{2}$$

$$h = \frac{4\pi}{\lambda} n \sin\left(\frac{\Theta}{2}\right), \tag{3}$$

where λ is the wavelength of the light in vacuum, n is the refractive index of the media of the suspension, and Θ is the scattering angle [23, 24]. In general, the scattered intensity (the reduced scattered intensity) is written in the form [24]

$$I(h) = KP(h)S(h) = KP\,, \tag{4}$$

with

$$k = \frac{4\pi}{\lambda} n. \tag{5}$$

For small scattering angles and scattering vectors, $P(h)$ in Eq. (4) can be written in the form of a serial expansion (Guinier) [2, 23]. By substituting this expansion of $P(h)$ and $S(h)$ into Eq. (4), and neglecting the higher-order terms, we obtain the well-known formula derived by Zimm with a multiplying factor of $(1+\cos\Theta)/2$ caused by the assumption of nonpolarized incident light (Eq. 6):

$$I = K^* c \left[1 - \frac{R_g^2}{3} k^2 \sin^2\left(\frac{\Theta}{2}\right) + \ldots\right] \times \left\{1 - \left[2B_2 + bk^2 \sin^2\left(\frac{\Theta}{2}\right)\right] c + \ldots\right\} \left(\frac{1+\cos\Theta}{2}\right), \tag{6}$$

where

$$B_2 = \frac{2\pi N_A}{M} \int_0^\infty \{1 - \exp[-V(r)/k_B T]\} r^2 \mathrm{d}r, \tag{7}$$

where N_A is the Loschmidt number and M is the mass of the particle, and the term $\exp[-V(r)/k_B T]$ is a probability approximation applied first by Raman [15, 16, 25] for the structure factor. $V(r)$ is the interparticle interaction pair potential in the dispersion. As one can see from Eq. (7), $1\text{-}\exp[-V(r)/k_B T]$ in the integral gives the probability of not finding another particle within distance r in the case of a repulsive potential. However, a statistical interpretation of Eq. (7) is possible only for special cases.

For a unit-volume cell the turbidity is defined by Eq. (8) [15, 16, 24]. The practical measurable physical amount is only proportional to that in Eq. (8) and is given by Eq. (9):

$$\tau^* = 2\pi \int_0^{\pi} I(\Theta) \sin\Theta \, \mathrm{d}\Theta, \tag{8}$$

$$\tau = \frac{\ln\left(\frac{I_0}{I_t}\right)}{l} = \frac{1}{V_s} \int_A \tau^* \, \mathrm{d}A, \tag{9}$$

where I_t and I_0 are the transmitted and incident intensity, respectively, l is the thickness of the sample, and A is the area illuminated. A finite volume of the sample is illuminated in the experiment, and the detector integrates over the illuminated area; therefore, the theoretical and the experimental quantities are only proportional to each other.

On the basis of the calculation presented by van Helden and Vrij [15], the turbidity depends on the particle concentration as presented in Eq. (10):

$$\begin{aligned} &\tfrac{c}{\tau^*} = b_0 + b_1 c + b_2 c^2 + \ldots, \\ &\tfrac{c}{\tau^*} = \tfrac{9}{4\pi K^*} \tfrac{1}{6 - R_g^2 k^2} \left[1 - \left(2B_2 - \tfrac{b}{2}k^2 - \tfrac{bR_g^2}{12}k^4 + \ldots\right)c + \ldots\right], \\ &\tfrac{b_2}{b_1} \approx B_2 + \tfrac{\pi}{3 N_A M} \int \{1 - \exp[-V(r)/k_B T]\} r^4 \mathrm{d}r \, k^2. \end{aligned} \tag{10}$$

From Eq. (10) the B_2 can be determined in two steps. The first measures the (linear) dependence of the turbidity on the particle concentration. The slope divided by the intercept of the turbidity versus the particle concentration function is an apparent coefficient. In the second step, the apparent coefficient versus k^2 (or λ^{-2}) gives B_2 as the zero-value intercept. This calculation eliminates any scaling factor that is present in the experimental value of the turbidity (Eq. 9) compared to the theoretical one (Eq. 8).

Materials and methods

Particles

The silica particles of about 50-nm diameter were prepared by the method of Stöber and Fink [12] and were kept in stock solvent until the experiments were performed. The solvent of the stock suspension was ethanol for the hydrophilic particles and toluene for the hydrophobic particles. The modification of the surface by stearyl alcohol has been described by van Helden et al. [26].

Organic liquids

Ethanol and toluene (Aldrich, laboratory grade) were dried on molecular sieve and centrifuged using a SORVAL RC5B supercentrifuge for 45 min (about 40,000g) in order to purify them from dust particles. The result was checked using photon correlation spectroscopy (PCS) measurements. Silica suspensions were prepared by diluting the stock dispersions and the purified solvents, and were ultrasonicated for 2 min. The samples were left for 24 h to reach adsorption equilibrium and were ultrasonicated for 1 min, 1 h before the measurements.

Electron microscopy

Electron microscopy was performed using a Philips CM-10 transmission electron microscope (TEM) at 100 kV with the samples on copper grids covered by Formvar film.

Nitrogen adsorption measurements

The specific surface area, a_s (BET-equation), was determined by measuring the adsorption of N_2 at 77 K in a Micromeritics Gemini 2375 automated gas sorption apparatus. Prior to the measurement, the powder samples were treated at 393 K for 2 h at a pressure of about 10^{-3} torr.

Adsorption excess isotherms

After equilibrating the samples for 24 h, the particles were settled out by centrifugation and the equilibrium of the supernatant, x_1, was determined using a Mach–Zender-type differential interferometer. The adsorption excess was calculated as a function of the equilibrium concentration:

$$n_1^{\sigma(n)} = \frac{n^0\left(x_1 - x_1^0\right)}{m},$$

where n^0 is the total molar amount of the solvent, m is the mass of the silica adsorbent, and x_1 and x_1^0 are the molar fractions of the ethanol after and before equilibrium [1, 2, 3, 4, 5, 6, 7].

Light scattering experiments

Light scattering measurements were performed using a Sematech Sem-633 stepper-motor-driven goniometer. The laser was a 3.5-mW He–Ne laser (wavelength 632.8 nm), polarized perpendicular to the plane of observation (and incidence). For PCS (dynamic light scattering) measurements a 12-channel R.T.G. logarithmic photon correlator was connected to the photomultiplier. The Rayleigh ratio of the dispersions was determined on the basis of the measured data compared to the scattered intensity of a reference sample (filtered benzene, original standard sample) with known Rayleigh ratio ($R_0 = 1.3\times10^{-5}$ cm^2) [27].

PCS measurements

PCS measurements were performed at different angles and the values of exponent of the intensity autocorrelation function, $\Gamma(h)$, were obtained by cumulant analysis [28].

Turbidity measurements

The turbidity was measured with a Uvicon-910 two-beam spectrophotometer, with air background in a quartz cell. The optics of the system allowed only the low-angle (less than 0.5°) part of the scattered light to enter the detector. The absorbance values measured were converted into turbidity using Eq. (9) and neglecting the absorption of the particles, i.e., assuming that all the attenuation of the light is caused by scattering.

Results and discussion

Silica particles

The specific surface area of the silica was 87.6 m^2g^{-1} for the hydrophilic particles and 43.7 m^2g^{-1} for the hydrophobic particles. Assuming that the particles are all separated, are spherical, and have a smooth surface, the particle radius was 17.2 nm for the hydrophilic particles and 34.5 nm for the hydrophobic particles. This result differs from the analysis of the TEM images (Fig. 2a). The average radius of the hydrophobic particles was 20–23 nm (Fig. 2b). This is in agreement with titration experiments [29], which showed that the silica particles have a microporous surface, and these pores can be blocked by the long-chain alcohol molecules used to modify the surface.

Stability of the silica dispersions

All the dispersions did not show changes in the kinetic stability during the time of the experiment; however, within about 12 h sedimentation of the hydrophilic particles was observed for $x_1 = 0.2$ ethanol concentration and at $x_1 = 0.3$ for the hydrophobic particles. This did not affect the experimental results, but indicated that the attraction between the hydrophilic particles increases with decreasing ethanol concentration and with increasing ethanol concentration for hydrophobic particles.

The adsorption-excess isotherm is presented in Fig. 3. The excess adsorption capacity was derived as $n_1^s = 1.485$ $mmolg^{-1}$ ethanol (hydrophilic particles) and $n_1^s = 0.554$ $mmolg^{-1}$, n_2^s 0.210 $mmolg^{-1}$ toluene (hydrophobic particles) [5, 6, 7]. Using these excess values, the specific surface area can be determined assuming an occupied area of the ethanol molecules of $a_{m1} = 120$ $mmolm^{-2}$ and of the toluene molecules of $a_{m2} = 180$ $mmolm^{-2}$. These specific areas are $a_L^s = 178.2$ m^2g^{-1} (hydrophilic particles) and $a_L^s = 104.3$ m^2g^{-1} (hydrophobic particles).

The autocorrelation function, $\Gamma(h)$, theoretically varies with the second power of h for particles moving with free diffusion and with the third power for particles trapped in a matrix and having vibration and rotational freedom. Martin and coworkers [17, 18, 19, 20] and Ren

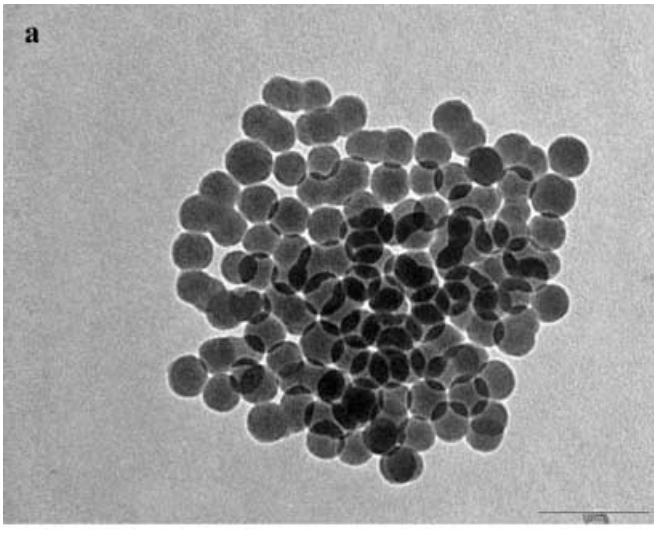

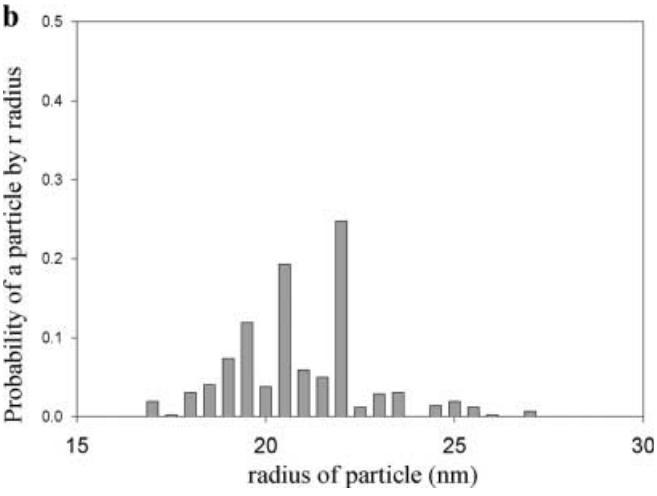

Fig. 2. **a** Transmission electron micrograph of silica particles, prepared by the method of Stöber, originally dispersed in ethanol. Average diameter 45 nm, the *bar* indicates 100 nm. **b** The size distribution function, determined from the electron micrographs

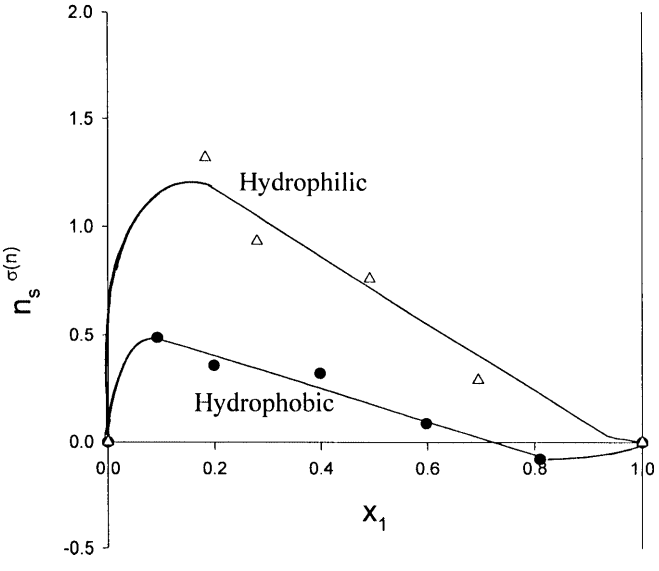

Fig. 3. Adsorption excess isotherms for the hydrophilic and the hydrophobic silica particles in ethanol–toluene binary mixtures

et al. [21] published results for silica dispersions showing noninteger power dependence, as the result of the fractal structure. In such a case, the classical interpretation of $\Gamma(h)$ is not applicable.

A representative logarithmic plot of Γ versus h is presented in Fig. 4. On fitting the data with a straight line, a characteristic noninteger power-law behavior was obtained from the slope for all the samples. The power of h varied between 2.2 and 2.7 (the slope in Fig. 4 is 2.67), which indicates a fractal structure of the aggregates. We did not perform further analysis of this data, because the lower scattering vector range, where free diffusion dominates, was not experimentally available in our system [17, 18, 19, 20, 21].

Because of the fractal properties, the dispersions can only be assumed as a steady-state system, but long-term kinetic and thermodynamic instability cannot be excluded [22].

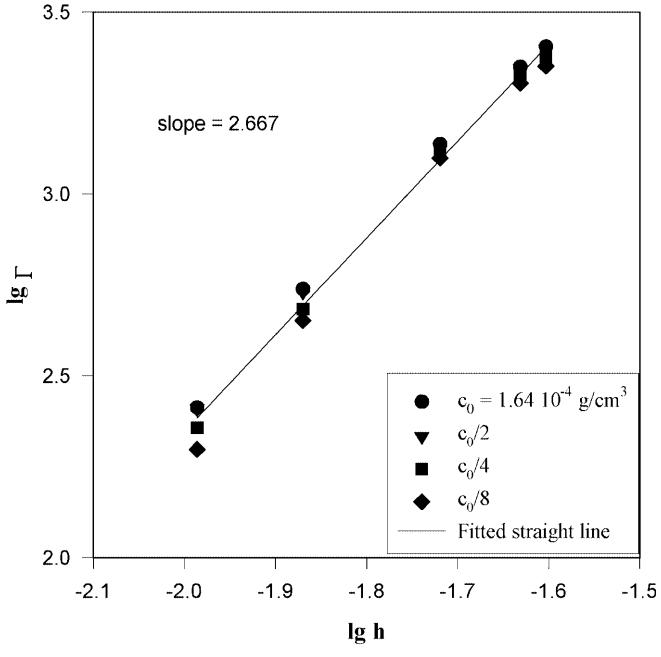

Fig. 4. The exponential decay, Γ, of the autocorrelation function as a function of the scattering vector, h, is a power law

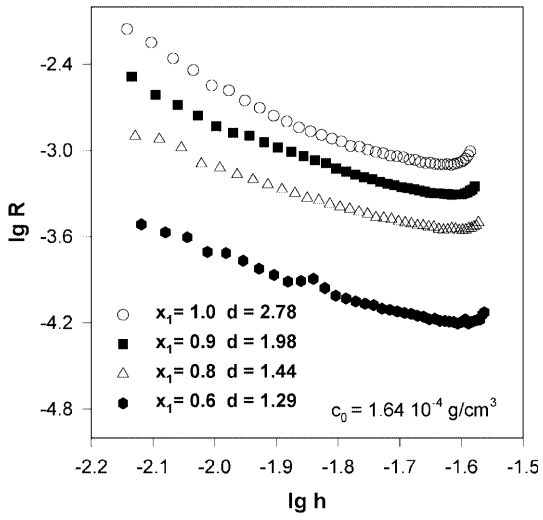

Fig. 5. Static light scattering curves in a log–log representation

Static light scattering experiments

To reveal the effect of the composition of the medium on the static light scattering curves, typical results are plotted at a fixed concentration ($c = 1.64 \times 10^{-4}$ gcm^{-3}) for the hydrophilic and hydrophobic particles in Fig. 5. In the log–log representation, the curves are straight lines, which indicates fractal behavior of the particle aggregations, in agreement with the dynamic light scattering study. The fractal dimension, d, of the particle aggregates can be determined as a function of both the particle concentration, c, and the mixture composition (characterized by the ethanol concentration, x_1). The limit of this analysis is that the inverse of the scattering vector, h^{-1}, must be in the range of the average size of the aggregates, R, and the radius of the building blocks of the structure, r. For the measurements presented h^{-1} was in the range of about 34 nm $< h^{-1} <$ 130 nm, which corresponds to clusters of 2–3 layers of particles.

Table 1 shows that the fractal dimension increases with increasing particle concentration: the structure of the aggregates varies from chainlike ($d = 1$) to space-filling ($d = 3$). For the hydrophobic particles, this trend is more pronounced at the highest alcohol concentrations. Accordingly, the slope $\Delta d/\Delta c$ is the highest in toluene for the hydrophobic particles, but the changes are smaller.

The changes in d with the medium composition are not very regular but the general trend is an increase in d with x_1 (hydrophilic particles). The stable dispersions ($x_1 \rightarrow 1$) with repulsive forces between the particles show space-filling clusters, whereas increasing attraction ($x_1 \sim 0.2$) causes more linear arrangements.

For the hydrophobic particles in the toluene-rich solvents space-filling structures are not formed. The structure approaches two-dimensional arrangements at $x_1 \geq 0.1$ up to the instability point ($x_1 \geq 0.3$).

To characterize how the fractal dimension varies with the particle concentration, a simple linear regression was applied, and the slopes $\Delta d/\Delta c$ (Table 1) of these regression lines are plotted as a function of the medium composition (ethanol concentration) in Fig. 6. This figure indicates a systematic trend; however, no quantitative model is available to interpret this behavior.

The attraction between the particles becomes stronger as the composition of the medium becomes less favored. ''Favored'' is used in the sense that the dis-

Table 1. Variation of the fractal dimension at different particle concentrations and mixture compositions for hydrophilic and hydrophobic silica particles. *Slope* denotes the slope of the fitted straight lines $d = f(c)$

Hydrophilic									
	d								
c (10^{-4} gcm^{-3})	$x_1 = 1.0$	c (10^{-4} gcm^{-3})	$x_1 = 0.9$	c (10^{-4} gcm^{-3})	$x_1 = 0.8$	c (10^{-4} gcm^{-3})	$x_1 = 0.6$	c (10^{-4} gcm^{-3})	$x_1 = 0.2$
0.20	1.50	0.20	1.20	0.41	1.30	1.64	1.29	1.64	1.15
0.41	2.04	0.41	0.95	0.82	1.33	3.27	1.46	3.27	1.26
0.82	1.71	0.82	1.77	1.64	1.44	6.54	1.68	6.54	1.26
1.64	2.78	1.64	1.98	3.27	1.39			13.08	1.35
Slope (cm^{3}g$^-$)	7,735		6,595		321		780		149
Hydrophobic									
	d								
c (10^{-4} gcm^{-3})	$x_1 = 0.0$	c (10^{-4} gcm^{-3})	$x_1 = 0.1$	c (10^{-4} gcm^{-3})	$x_1 = 0.2$	c (10^{-4} gcm^{-3})	$x_1 = 0.3$		
0.31	1.27	2.50	1.58	1.25	1.88	2.50	1.57		
1.25	1.42	5.00	1.83	5.00	1.94	5.00	1.62		
2.50	1.49	10.00	2.20	10.00	1.90	10.00	1.82		
						20.00	1.97		
Slope (cm^{3}g$^-$)	993		825		25		231		

persion shows higher kinetic stability. This property can be generally correlated with the wetting abilities of the medium toward the surface of the particles [1, 2, 3, 22].

Second virial coefficient

The turbidity at different medium compositions is presented in Fig. 7 for a particle concentration of 10^{-3} gcm^{-3}. In the direction of the instability range ($x_1 = 0.2$–0.3 liquid mixture composition) for hydrophilic and hydrophobic particles the turbidity decreases. An example of the apparent second virial coefficients, calculated from the turbidity data, as a function of λ^{-2} is shown in Fig. 8. A second-order polynomial or linear fitting was applied to calculate the second virial coefficient on the basis of Eq. (10). $B_2(x_1)$ (Fig. 9) increases as the concentration of the nonpolar solvent increases (x_1 decreases) for the hydrophilic particles, in analogy, it increases when x_1 increases for hydrophobic particles. This variation correlates with the increasing attraction between the particles. When the medium becomes less favored (corresponding to a reduced solvency in polymer chemistry) B_2 increases and the stability decreases.

Conclusions

Aggregation of silica particles was investigated by static and dynamic light scattering. Even in the stable dispersions the particles were not equally distributed. The data indicate that the aggregates are of fractal type, and the fractal dimension varied with the concentration of the particles and the composition of the medium. For both the hydrophilic and the hydrophobic particles there is a mixture composition where the changes of the fractal dimension with the particle number is a minimum. This

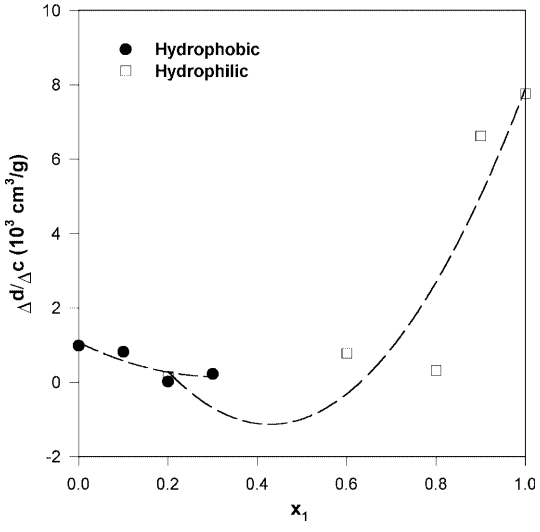

Fig. 6. Changes of the mass fractal dimension with the particle concentration at different compositions of the medium

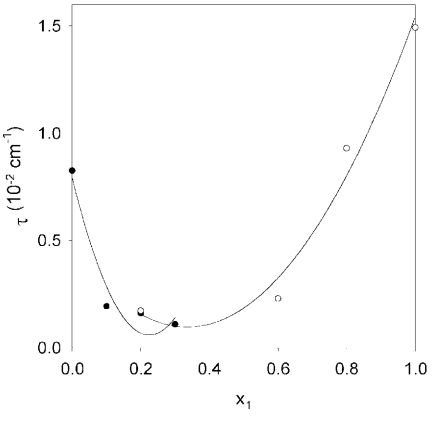

Fig. 7. Turbidity of silica particles at a particle concentration of 10^{-3} gcm^{-3} for different ethanol–toluene mixtures

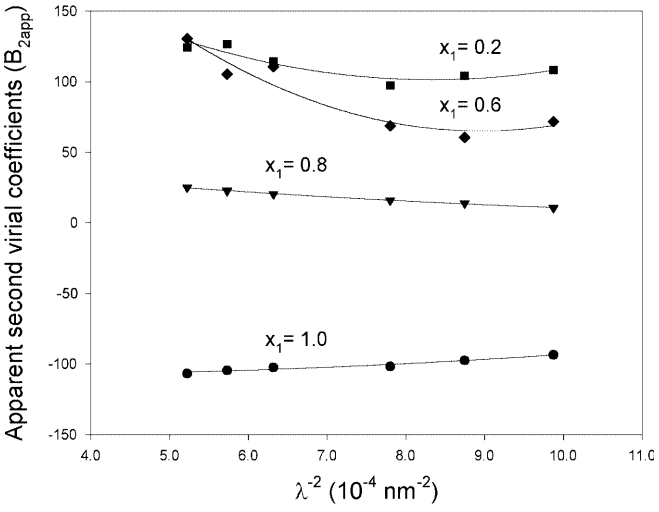

Fig. 8. The apparent second virial coefficient, B_2, as a function of the wavelength of the light

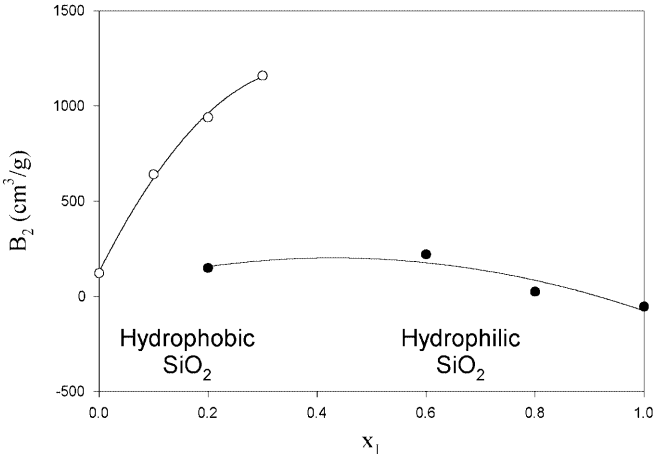

Fig. 9. The second virial coefficients, from turbidity measurements, as the function of the composition of the medium

Table 2. Qualitative comparison of the stability, the second virial coefficients, and the fractal properties for the hydrophilic and hydrophobic silica particles in the different ethanol–toluene mixtures

x_1	Stability		Virial coefficient (B_2, cm^{3}g^{-1})		Fractal properties slope of $d(c)$ (cm^{3}g^{-1})	
	Hydrophilic	Hydrophobic	Hydrophilic	Hydrophobic	Hydrophilic	Hydrophobic
0.0	Unstable	Stable	–	122	–	993
0.1	Unstable	Good	–	641	–	825
0.2	Low	Good	149	941	149	25
0.3	Low	Unstable	–	1,160	–	231
0.6	Good	Unstable	221	–	6,595	–
1.0	Stable	Unstable	–53	–	7,735	–

case is considered to occur when the interparticle attraction is the highest. To characterize this property, both the linear slope of the fractal dimension versus the particle concentration and the second virial coefficient (obtained from experimental turbidity data) were derived. The two independent parameters show a similar variation with the mixture composition for both types of suspensions, containing hydrophilic or hydrophobic particles (Figs. 6, 9, Table 2).

A more detailed study of the correlation of the three properties – the stability, the second virial coefficients, and the particle-concentration-dependent fractal dimension – would only be possible using numerical dynamic modeling.

Acknowledgements The authors would like to thank the support of the Hungarian Research Fund: OTKA T 025392, and to Professor Dr. Gerhard Lagaly for his valuable discussion and advices.

References

1. Schay G (1965) In Matijevic E (ed) Surface and colloid science, vol 2. Wiley, London, p 155
2. Kipling JJ (1965) Adsorption from solutions of non-electrolytes. Academic, New York
3. Schay G (1969) In Everett DH (ed) Surface area determination. Proceedings of the international symposium. Butterworths, London, p 273
4. Schay G (1976) Pure Appl Chem 48:393–400
5. Dékány I (1993) Pure Appl Chem 65:901-906
6. Dékány I, Turi L (1998) Colloids Surf A 133:233–243
7. Machula G, Dékány I, Nagy LGY (1993) Colloids Surf A 71:241–254
8. Dékány I, Nagy I, Turi L, Király Z (1996) Langmuir 12:3709–3715
9. Király Z, Turi L, Dékány I, Bean K, Vincent B (1996) Colloid Polym Sci 274:779–787
10. Vincent B (1973) J Colloid Interface Sci 42:270–285
11. Vincent B, Király Z, Emmett S, Beaver A (1990) Colloids Surf 49:121–132
12. Stöber W, Fink A (1968) J Colloid Interface Sci 26:62-69
13. Dékány I, Haraszti T, Turi L, Király Z (1998) Prog Colloid Polym Sci 111:65–73

14. Vrij A, Jansen JW, Dhont JKG, Pathmamanoharan C, Kops-Werkhoven MM, Funaut HM (1983) Faraday Discuss Chem Soc 76:19–35
15. van Helden AK, Vrij A (1980) J Colloid Interface Sci 78:312
16. Israelachvili JN (1985) Intermolecular and surface forces with applications to colloidal and biological systems. Academic, New York
17. Martin JE, Hurd AJ (1987) J Appl Crystallogr 20:61–78
18. Martin JE (1987) Phys Rev A 36:3415
19. Martin JE, Ackerson BJ (1985) Phys Rev A 31:1180
20. Martin JE (1986) J Appl Crystallogr 19:25–27
21. Ren SZ, Tombácz E, Rice JA (1996) Phys Rev E 53:2980
22. Rajagopalan R, Heimenz PC (1997) Principles of colloid and surface chemistry, 3rd edn. Dekker, New York
23. Glatter O, Kratky O (1982) Small angle X-ray scattering. Academic, New York
24. Kerker M (1969) The scattering of light and other electromagnetic radiation. Academic, New York
25. Guinier A, Fournet G (1955) Small-angle scattering of X-rays. Wiley, New York
26. van Helden AK, Jansen JW, Vrij A (1981) Colloid Interface Sci 81:354
27. Sematech (1994) Sematech SEM-633 users manual. Sematech GmbH
28. Pecora R (1985) Dynamic light scattering. Applications of photon correlation spectroscopy. Plenum, New York
29. Szekeres M, Tóth J, Dékány I (2002) Langmuir (accepted)